coatings

MDPI

*Article*

# Durability of Acrylic Cataphoretic Coatings Additivated with Colloidal Silver

**Massimo Calovi and Stefano Rossi ***

Department of Industrial Engineering, University of Trento, 38123 Trento, Italy; massimo.calovi@unitn.it
* Correspondence: stefano.rossi@unitn.it; Tel.: +39-0461-282442

**Abstract:** In this work, colloidal silver has been added into an acrylic clear cataphoretic bath, evaluating the effect of two different filler amounts on the durability of the composite coatings. The three series of samples were characterized by electron microscopy to assess the possible change in morphology introduced by the silver-based additive. The protective properties of the coatings were evaluated by a salt spray chamber exposure and electrochemical impedance spectroscopy measurements, evidencing the negative effect provided by high amount of silver, which introduced discontinuities in the acrylic matrix. Finally, the durability of composite coatings was studied by exposing them to UV-B radiation, observing a strong phenomenon of silver degradation. Although the coating containing high concentrations of silver demonstrated poor durability, this study revealed that small amounts of silver can be used to provide particular aesthetic features, but also to improve the protective performance of cataphoretic coatings.

**Keywords:** colloidal silver; cataphoretic deposition process; salt spray chamber; electrochemical impedance spectroscopy; UV-B exposure test



**Citation:** Calovi, M.; Rossi, S. Durability of Acrylic Cataphoretic Coatings Additivated with Colloidal Silver. *Coatings* **2022**, *12*, 486. https://doi.org/10.3390/coatings12040486

Academic Editor: Mohammadreza Daroonparvar

Received: 14 March 2022
Accepted: 3 April 2022
Published: 4 April 2022



## 1. Introduction

Among the various deposition processes of organic coatings, cataphoresis represents an innovative method of particular industrial interest. The typical spray process, in fact, can be applied to different substrates, in addition to metal alloy [1–3], such as glass, paper, and cotton fabric [4], but it has always exhibited technical limitations. For example, the control of the thickness of the layer, as well as the geometry of the component to be coated, are critical aspects during spraying. Differently, cataphoresis has shown several interesting features over the years. The electrodeposition process enables the creation of organic layers with high adhesion and corrosion protection properties [5,6], which are also applicable on products with complex geometry [7]. Thanks to the polarization of the sample that occurs during the electrodeposition, the electric field allows one to achieve a uniform coverage on the surface to be coated. Furthermore, from an industrial point of view, cataphoresis is highly appreciated, as it represents a simple, fast, and cost-effective method to produce large-scale industrial coatings, with a low-environmental impact [8].

Thanks to these aspects, cataphoresis is often successfully employed in the automotive industry [9–11], but in recent years it has also aroused particular interest in the research-academic field. In fact, several works have turned to the optimization of the process equipment [12,13] and parameters, such as the curing temperature [14] and the deposition voltage [15], in order to further improve the behavior of the cataphoretic layers. The electrodeposition process has exhibited high versatility, as it has been applied to different metal substrates, such as Zn-Mg alloys [16,17], Ti-Mo alloy [18], aluminum alloys [19–21], and steel alloys [22]. Furthermore, this method has also been evaluated in synergy with different types of pre-treatments [23,24] to improve the adhesion and durability of the coating. Recently, several scientists have focused on the study of the implementation of the cataphoretic organic matrix with different types of fillers, in order to obtain multifunctional

composite coatings. The protective performances, for example, have been further improved by adding cerium-based nanoparticles [25,26], or thanks to functionalized graphene oxide flakes [27–30]. Furthermore, the aesthetic features obtainable from cataphoresis by incorporating particular thermochromic pigments were also evaluated [31], which compared the results with the behavior of the typical spray process [32].

A current trend topic in the world of organic coatings is represented by the addition of silver-based fillers [33–35]. This phenomenon is mainly due to the escalation of the SARS-CoV-2 pandemic, which has led scientific research to seek a solution to the spread and transmission of pathogenic microorganisms through surface contamination. The pandemic has in fact highlighted how the continuous surface disinfection is not sustainable, in terms of temporal and economic efforts [36]. The simplest and most effective alternative approach lies precisely in functionalizing the surfaces by adding silver, whose successful biocidal effect has been amply demonstrated over the last 25 years [37–40]. Silver ions, adhering to the cell wall and modifying its permeability, are able to deactivate respiratory enzymes and hinder DNA replication [41,42]. Thus, silver is commonly employed in sensitive health application that requires extreme hygiene, such as artificial implants, surgical instruments, and dental implants [43], or in food and textile industries [40]. Thus, in order to realize multifunctional surfaces with antibacterial features, silver has recently been subjected to much research on its antimicrobial [44], bioactive activities [45], and cytotoxicity features [46].

Silver has been applied to different types of surfaces. Anodized aluminum layers have shown good compatibility with different types of silver-based fillers, confirming excellent antibacterial performance [47–49]. Furthermore, antimicrobial silver has been encapsulated in $TiO_2$ coatings [50] and $TiO_2$ nanotubes [51], deposited on cotton fabric [52], and implemented in a Mg-Al layered double hydroxide coating [53].

Consequently, the world of paints has also been recently affected by these studies [54–58]. For example, Lateef et al. [59] investigated the efficiency of silver nanoparticles (AgNPs) as an antibacterial additive for enamel paint, while Deyà et al. [60] and Barberia-Roque et al. [61] studied the bactericidal effect of silver in acrylic water-based paint. Similarly, Liu et al. [62] explored the in situ synthesis of AgNPs in transparent PVA films for antibacterial purpose. The biocidal activity of AgNPs in polyurethane coating was assessed by Bechtold et al. [63], who confirmed the good efficiency of silver against bacteria but, at the same time, the non-satisfactory resistance against fungi. On the other side, Asafa et al. [64] reported the influence of AgNPs on physical and mechanical properties of emulsion paint, comparing the results with the behavior of ZnO and $Fe_2O_3$ additives. Finally, the antibacterial properties of silver in emulsion paint was also assessed by Ohashi et al. [65], who evidenced a better paintability and transparency of silver–cytokinin complex filler for emulsion paint compared to a commercialized paint filler.

However, despite the great interest of the paint industry in silver-based additives, the literature does not offer any study on the synergy between cataphoresis and silver. The high process yields of cataphoresis, combined with the excellent covering power of the electrodeposited layers and their compactness, makes this method one of the most promising for the production of organic matrix composite coatings incorporated with silver-based filler. Thus, the purpose of this work is to evaluate the effect of colloidal silver on the durability of acrylic cataphoretic coatings. Two different amounts of colloidal silver were added into the cataphoretic bath, to assess how the silver concentration influences the coatings' performance. The study employed an acrylic top-coat cataphoretic bath, as it did not contain pigments and additives that could influence the effect and behavior of colloidal silver.

The samples were characterized by means of the scanning electron microscope (SEM), to observe the morphology of the deposited composite coatings by studying the influence of the silver additive. The effect of the amount of silver on both corrosion resistance performance and behavior in the aggressive environment of the acrylic-based coatings were assessed by subjecting the samples to electrochemical impedance spectroscopy mea-

surements (EIS) and exposing them in the salt spray chamber, respectively. Finally, the durability of the samples and consequent aesthetic performance were evaluated with the UV-B exposure.

## 2. Materials and Methods

### *2.1. Materials*

The colloidal silver (65–75 wt.% Ag) and acetone were supplied from Sigma-Aldrich (St. Louis, MO, USA) and used as received. The 40 × 70 × 2 $mm^3$ carbon steel substrate (Q-panel type R (0.15 wt.% C-Fe bal.) was supplied by Q-lab (Westlake, OH, USA). The cataphoretic bath Arsonkote 202 Acy Cata W202 × 30 was provided by Arsonsisi (Milan, Italy). This industrial product is based on modified acrylic resin, with glycols employed as the solvent. It possesses a dry residue (after 2 h at 120 °C) equal to 28–30%, and a specific weight of 1.00–1.20 g/$cm^3$.

### *2.2. Deposition of Acrylic–Ag Coatings*

The carbon steel substrates were subjected to a degreasing process in acetone, supported by ultrasonic agitation, followed by a sandblasting step with corundum powder (0.2 mm diameter, 70 mesh). The sandblasting process introduced a roughness [Ra] equal to 3.05 ± 0.22 µm in the steel substrates. Finally, the steel plates were further degreased in acetone, in order to remove possible traces of contamination.

The deposition setup was set in a 200 mL acrylic cataphoretic bath. A 300 × 50 $mm^2$ flat stainless steel plate, used as the anode, was placed in front of the sample, at a distance of 80 mm. As colloidal silver granules are soluble in water, they were added directly to the cataphoretic bath, because it is water-based. Two different amounts of colloidal silver were added into the bath, which was stirred for 30 min with an ultrasound probe, to facilitate the complete dissolution of the colloidal silver granules. Both the two sets of samples were deposited, keeping constant all the process parameters, to better compare the coating behavior. The electrodeposition was carried out at a voltage of 75 V for 120 s, followed by a curing step in an oven at 140 °C for 45 min, as suggested by previous studies [29,30]. The sample production process is outlined in Figure 1.

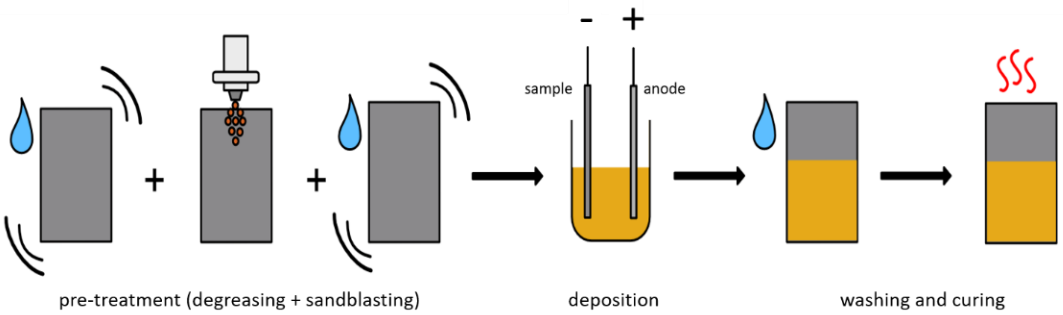


**Figure 1.** Scheme of the sample production process.

The performances of the two series of acrylic–Ag samples were compared with the behavior of a pure acrylic layer, free of filler. The three samples series are summarized in Table 1 with the sample nomenclature.

**Table 1.** Labeling of samples with different colloidal silver concentration.

| Bath | Colloidal Silver Concentration (wt.%) | Sample Nomenclature |
|---|---|---|
| Clear coat | 0.00 | A |
| | 0.05 | A1 |
| | 0.10 | A2 |

The two silver concentrations, shown in Table 1, were chosen because they achieved enough silver quantity in the coating in order to guarantee good antibacterial performances, as highlighted in the literature [48]. The real amount of silver detected inside the two coatings A1 and A2 are introduced later, in paragraph 3.1.

### *2.3. Characterization*

The optical stereomicroscope Nikon SMZ25 (Nikon Instruments, Amstelveen, the Netherlands) and low vacuum scanning electron microscope SEM JEOL IT 300 (JEOL, Akishima, Tokyo, Japan) were employed to analyze the surface morphology of the coatings, with the aim of verifying whether the introduction of colloidal silver has influenced the electrodeposition process, modifying its yield and introducing defects in the acrylic matrix. An energy-dispersive X-ray spectroscopy (EDXS, Bruker, Billerica, MA, USA) analysis has also been carried out in order to map the silver distribution in the coatings. Finally, the thickness of the three series of composite coatings was measured by means of the Phynix Surfix digital thickness gauge (Phynix, Neuss, Germany).

The samples were exposed in a salt spray chamber (Ascott Analytical Equipment Limited, Tamworth, UK) for 500 h, following a ASTM B117-11 standard [66] (5 wt.% sodium chloride solution), to assess the corrosion protection behavior of the coatings in a particular aggressive environment. The adhesion of the coatings was evaluated by means of a mechanical cut made on the surface of the samples, analyzing the possible detachment and water uptake phenomena.

The protective features of the composite coatings were studied by means of Electrochemical Impedance Spectroscopy (EIS) measurements, carried out with a potentiostat Parstat 2273 (Princeton Applied Research by AMETEK, Oak Ridge, TN, USA) with the software PowerSuit ZSimpWin (version 2.40) and applying a signal of about 15 mV (peak-to-peak) amplitude in the $10^5$–$10^{-2}$ Hz frequency range. The cell setup mas composed of an Ag/AgCl reference electrode (+207 mV SHE) and a platinum counter electrode, immersed in the 3.5 wt.% sodium chloride solution. The samples were kept immersed in the test solution for a total of 500 h, with a testing area equal to 6.15 $cm^2$.

Finally, UV-B exposure tests were carried out at 313 nm for 500 h, using an UV173 Box Co.Fo.Me.Gra (Co.Fo.Me.Gra, Milan, Italy) and following the ASTM G154-16 standard [67]. The chemical–physical degradation of the coatings was analyzed with a Konica Minolta CM2600d, spectrophotometer (Konica Minolta, Chiyoda, Tokyo, Japan) using a D65/10° illuminant/observer configuration in SCI mode, evaluating visual-aesthetical variations.

## 3. Results

### *3.1. Coating Morphology*

The deposition of the acrylic–Ag composite coatings took place by adding the clear cataphoretic bath with colloidal silver. The silver-based additive is in the form of a greyish powder, with a very variable size, as shown in Figure 2. In fact, the size of the granules varies from a few μm, up to over 200 μm.

However, this aspect seems not to be relevant for the electrodeposition process, as colloidal silver powders are completely soluble in water. Consequently, once added to the cataphoretic bath, composed of 60 wt.% of water, the powders did not reveal macroscopic aggregation phenomena. Previous works have highlighted the strong criticalities in adding fillers in cataphoretic baths: the reaction with the polymeric matrix often results in aggregation phenomena of the fillers with consequent defects in the coatings [29,30]. Otherwise, colloidal silver apparently represents an ideal candidate as an additive in cataphoretic depositions.

Dissolving in water, the colloidal silver powders create a yellow-orange color solution. Consequently, the color of the cataphoretic bath also varies according to the quantity of the introduced colloidal silver. The hue of the electrodeposition bath, from transparent, varies towards an orange tone, becoming darker and darker with the increase in the colloidal silver amount. Figure 3 faithfully represents this phenomenon: the three types of samples

studied in this work exhibit different aesthetic features due to the presence of colloidal silver. Sample A has a clear coating of pure acrylic matrix, free of additives. On the other hand, samples A1 and A2 reveal a yellow and orange coating, respectively, the tones of which strongly depend on the concentration of the silver-based filler. The coloring of the composite layers appears homogeneous and constant over the entire surface, proof of the high aesthetic efficiency and covering power of cataphoresis [32].

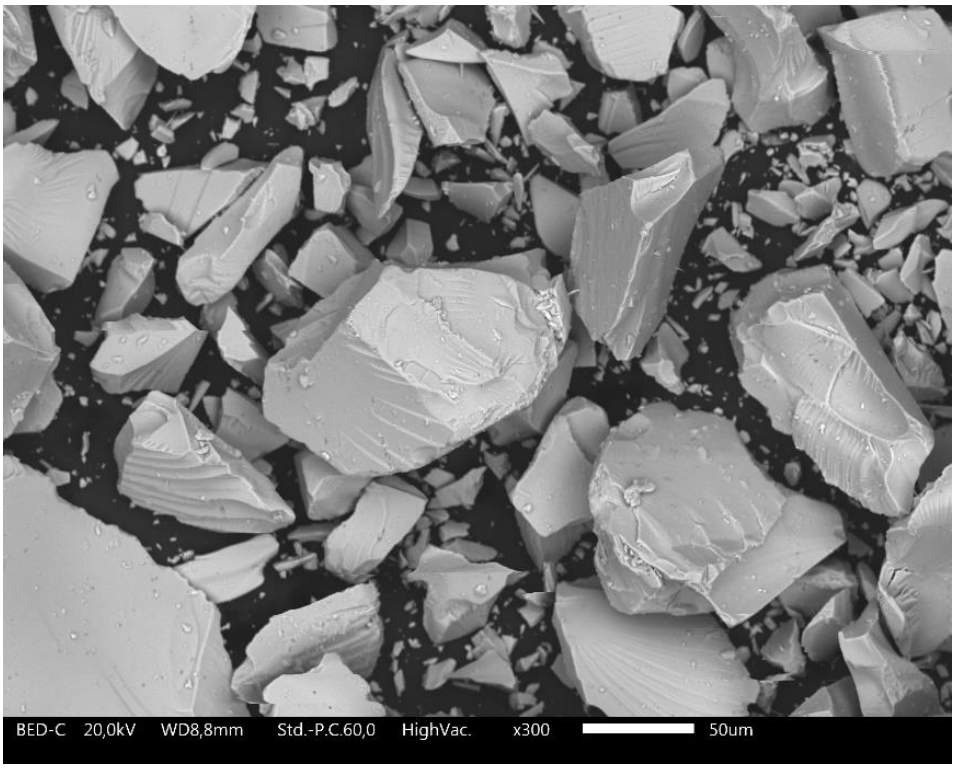


**Figure 2.** Colloidal silver acquired by SEM.

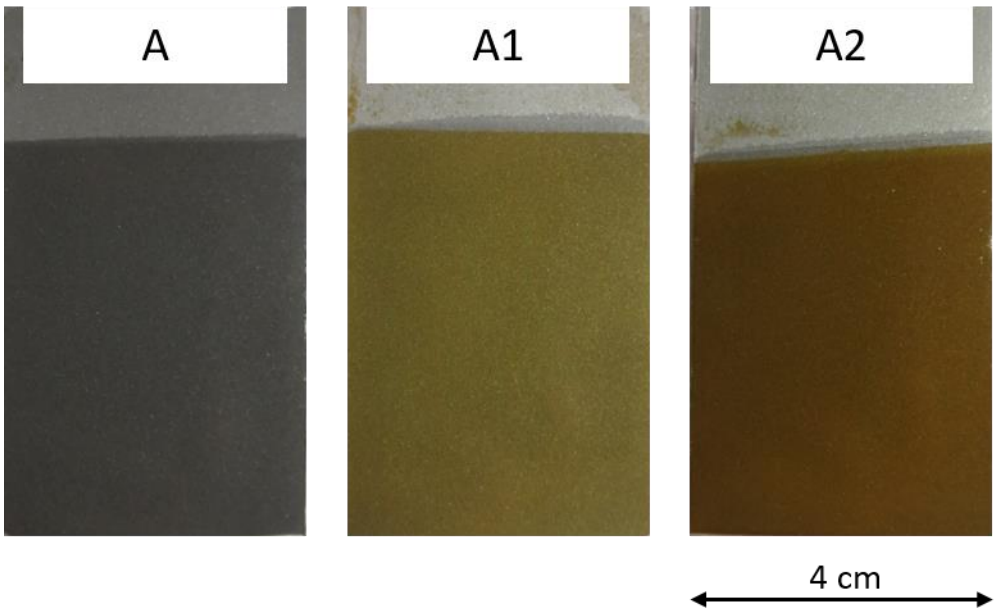


**Figure 3.** Photograph of the three as-made sample series, where A represents the coating of pure acrylic matrix, while A1 and A2 were deposited by introducing 0.05 wt.% and 0.10 wt.% of colloidal silver in the cataphoretic bath, respectively.

Although the three series of samples exhibit different appearance from each other, the thickness of the coatings is comparable. Table 2 shows the coatings thickness measured with the digital thickness gauge: the values constitute the average of 50 measurements performed on 5 samples (10 measurements per sample) for each series.

**Table 2.** Coatings thickness of the three series of samples.

| Sample | Thickness [μm] | St. Dev. [μm] |
|---|---|---|
| A | 22.2 | 0.8 |
| A1 | 23.4 | 1.0 |
| A2 | 21.7 | 1.3 |

The obtained thickness values are in accordance with the usual outcome achieved with cataphoretic process, as confirmed by the literature [9]. The results suggest that the addition of colloidal silver to the cataphoretic bath did not affect the process yield of the electrodeposition. The samples show a compact and homogeneous coating, free from macroscopic defects. This outcome reinforces the previous assumptions relating to the efficient use of colloidal silver as an additive in cataphoretic baths. Furthermore, the introduction of colloidal silver in the acrylic bath did not affect the leveling power of the cataphoretic process, as all the three series of coatings exhibit a particularly smooth coating, whose roughness [Ra] is comparable and equal to 0.25 ± 0.03 μm.

Thus, the three series of coatings were observed by SEM, in order to better analyze their morphology and highlight possible microscopic defects. Figure 4 shows the micrographs of the surfaces of the three samples, acquired by SEM.

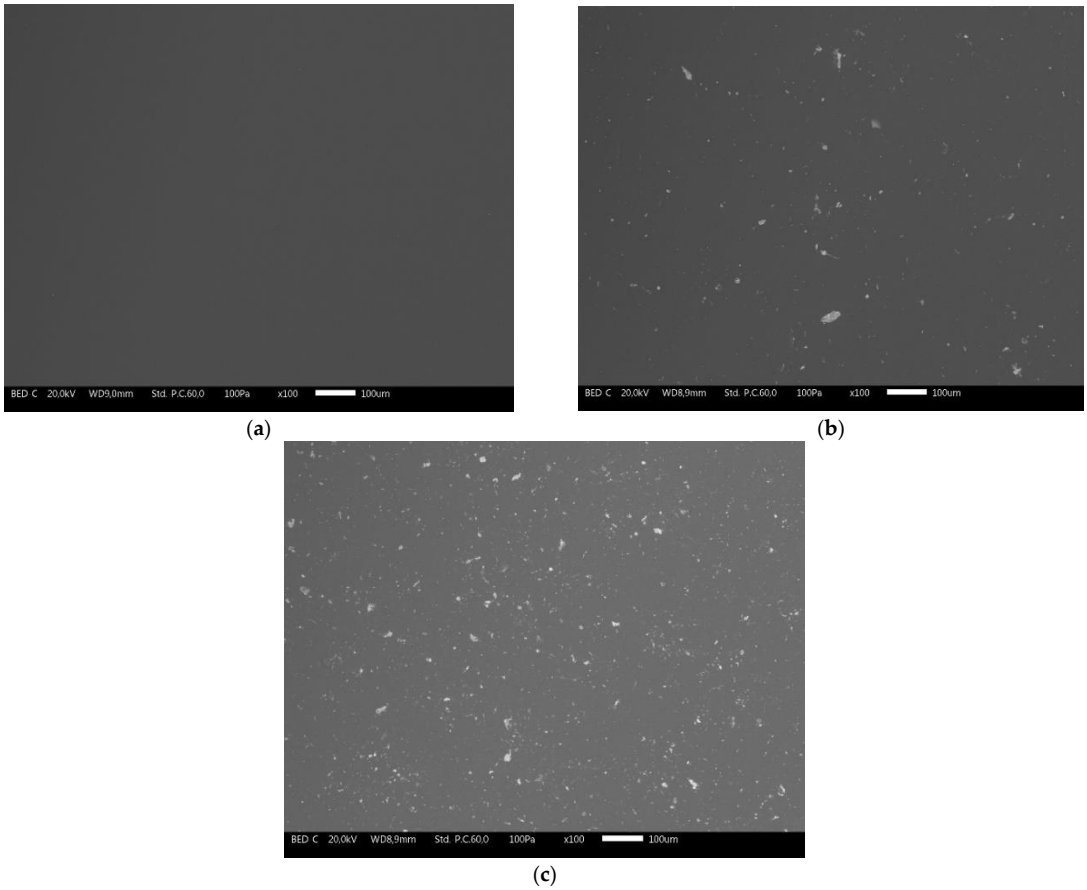


(**a**) (**b**) (**c**)

**Figure 4.** SEM micrograph of the surface of sample A (**a**), sample A1 (**b**) and sample A2 (**c**), respectively.

Coating A (Figure 4a) appears completely homogeneous. Morphological defects, such as bubbles in the acrylic matrix, cannot be appreciated. In contrast, the coatings of samples A1 and A2 (Figure 4b,c, respectively) reveal different light-colored traces homogeneously distributed on their surface. The amount of these traces increases from sample A1 to sample A2, suggesting that they are closely related to the addition of colloidal silver to the acrylic bath. Despite the presence of this phenomenon, no appreciable defects are observed even in coatings A1 and A2. Therefore, although silver is conductive, once introduced into the cataphoretic bath it does not influence the electrodeposition process through the development of eddy currents, as observed, for example, with graphene-based filler [29].

In order to confirm the nature of the clear traces, the samples were examined by EDXS investigation. The EDXS analysis revealed a concentration equal to 1.4 wt.% and about 3 wt.% of silver on the surface of the samples A1 and A2, respectively. Figure 5 shows, as an example, a micrograph of the surface of the sample A1, with the respective EDXS map of the Ag element. Indeed, the clear traces observed by SEM are representative of the presence of silver. Although silver is effectively distributed over the entire surface of the coatings in a homogeneous way, in some cases it is possible to notice a thickening of silver whose dimensions exceed 20 μm. The morphology of these clusters differs from the powders shown in Figure 2. Consequently, it is likely that the colloidal silver actually dissolved in water, but was subsequently subjected to thickening phenomena in the acrylic matrix. In fact, colloidal silver itself is not compatible with polymeric matrices, if not first effectively dissolved in water. It is therefore probable that the interaction between the silver–water solution and the acrylic resin in the cataphoretic bath has caused the undesired phenomena of silver re-accumulation. This, in fact, represents the only real noteworthy defect due to the addition of colloidal silver.

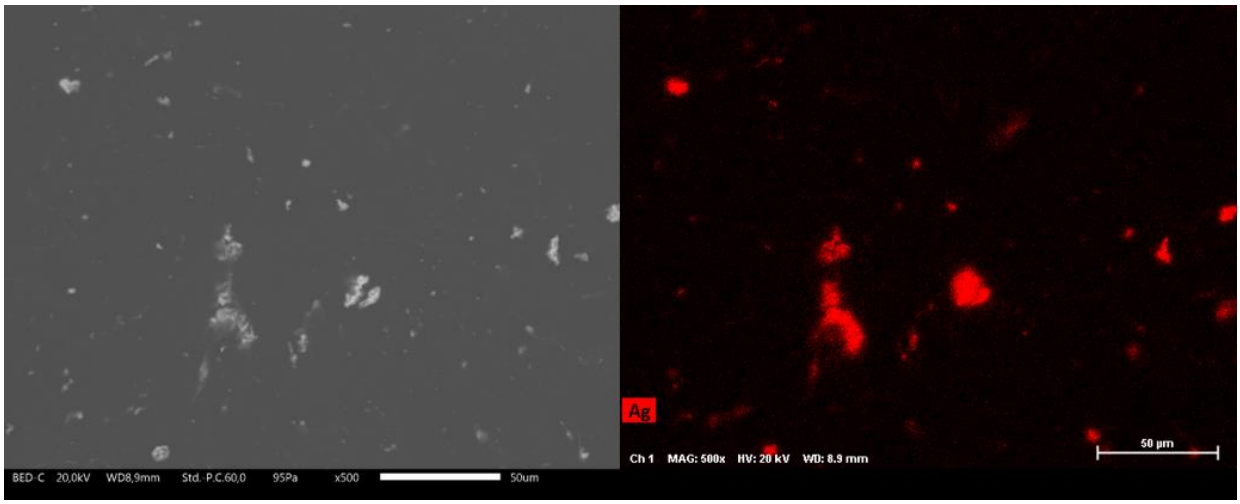


**Figure 5.** SEM micrograph of the surface of sample A1, with relative EDXS map of Ag element.

Thus, the effect of this phenomenon on the protective performances of the acrylic matrix was subsequently evaluated by exposing the coatings in aggressive environments and by means of suitable electrochemical techniques.

### *3.2. Salt Spray Chamber*

The three series of samples were exposed in the salt spray chamber for a total of 500 h. During the first 100 h of exposure the coatings were observed every 24 h, after which they were monitored every 100 h, until the end of the analysis. An artificial cut of 1 mm width was realized on the surface of the coatings, to create a mechanical defect in the cataphoretic layer, forcing the development of corrosive phenomena at the substrate-coating interface. Thus, the evolution of blisters, due to water uptake from to the artificial notch, and the coatings' adhesion level were visually evaluated [68].

Figure 6 shows the evolution of the coatings' degradation during the exposure in the salt spray chamber. All three series of coatings exhibit a halo around the central notch after 100 h of exposure. This phenomenon, together with the development of blisters, is symptomatic of water absorption in correspondence of the artificially introduced defect. The samples exhibit a comparable behavior, except for the greater blister evolution observed in coating A2. At the end of the test (500 h), the entire surfaces of the three coatings are covered with blisters. However, it must be considered that cataphoresis is normally used as a primer or as a finishing layer in non-aggressive environments, while the exposure test in salt spray chamber exhibits a high degree of aggressiveness. The absorption of the aggressive solution within the cataphoretic layers is associated to their adhesion levels: the greater the distance of the blister from the central notch, the lower the adhesion of the coatings. Again, it is difficult to differentiate between the behavior of the three samples, as the penetration of the test solution caused the development of blisters over the entire surface of the coatings.

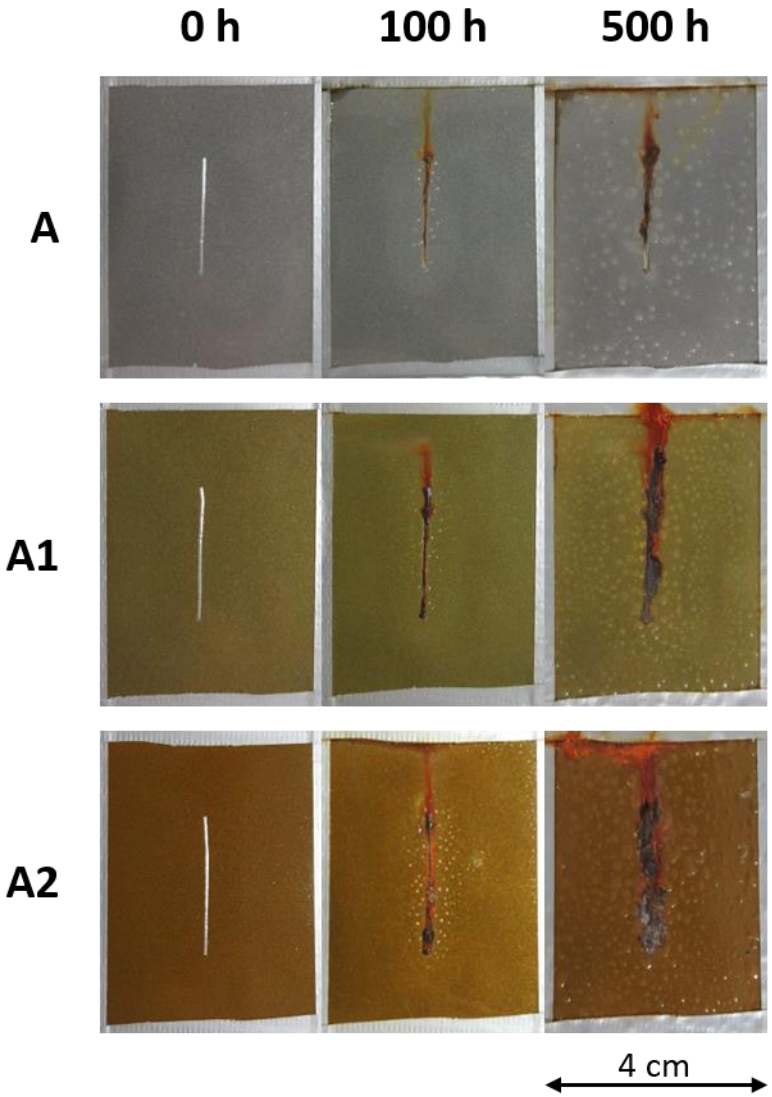


**Figure 6.** Coating degradation during sample exposure in salt spray chamber.

To better observe the phenomena that took place close to the artificial notch, the corrosion products developed on the coatings were removed by stirring the samples in citric acid solution (pH = 3) for 2 h. Thus, the samples were analyzed by stereomicroscope observations, as shown in Figure 7. According to the standard [66], an organic coating with good adhesion to the substrate should show maximum detachment from the notch area

of about 1000 µm. Following this definition, all three series of coatings possess excellent adhesion, typical of a cataphoretic layer, as they did not exhibit clear detachment of the coating caused by water absorption or development of corrosion products. However, in some spots it is possible to appreciate the detachment of the layers from the metal substrate in proximity of the notch: this phenomenon is represented by lighter blisters (clearly evident above all in Figure 7a,b). This occurrence sometimes exceeds the limit of 1000 µm, but it is a detachment of the layer strictly linked to the evolution of the blister, therefore not fully considered by the standard [66].

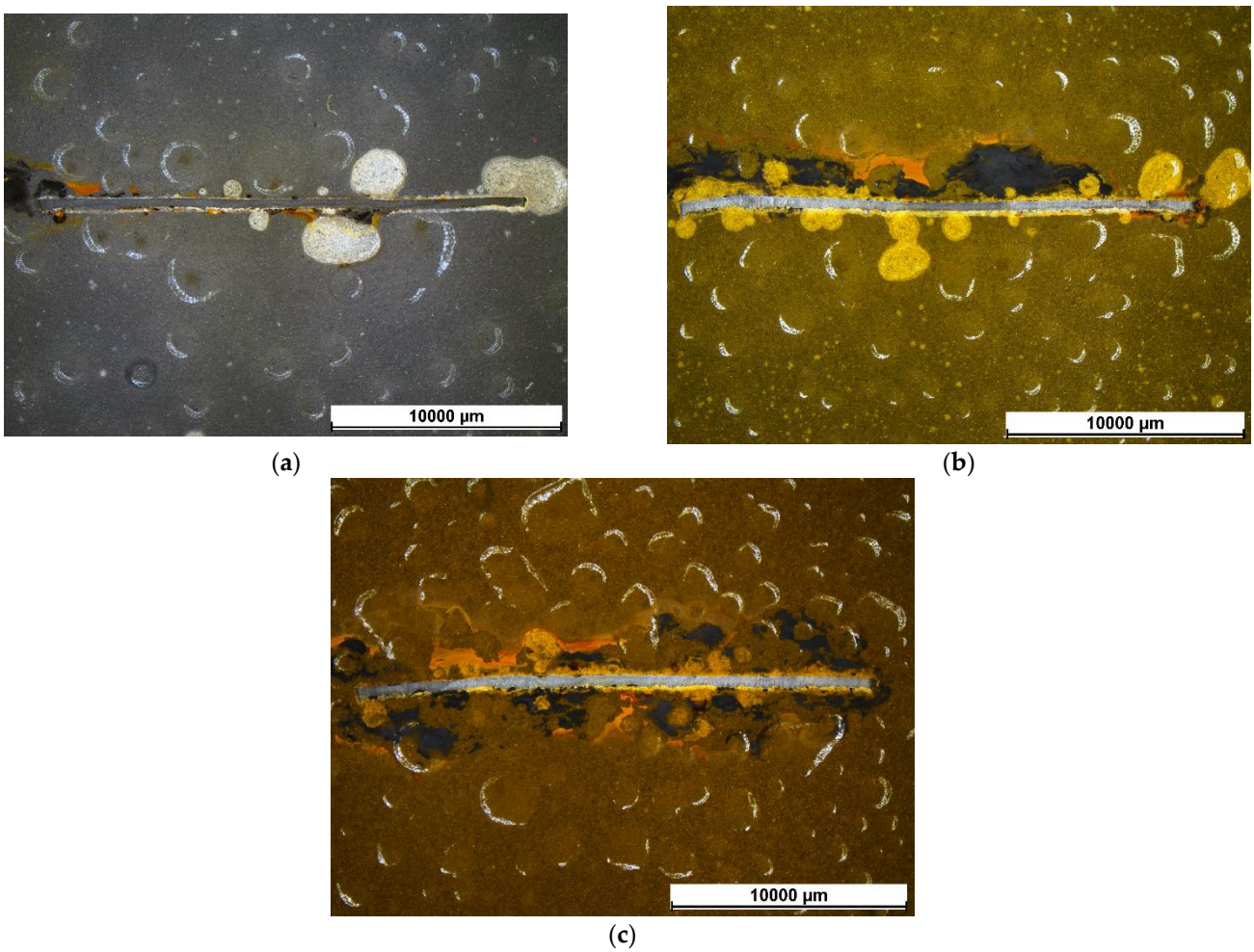


**Figure 7.** Samples A (**a**), A1 (**b**), and A2 (**c**) appearance after 500 h of exposure in the salt spray chamber.

The density of blisters, rather than their average size, represents the aspect that most differentiates the three series of samples. As can be observed from the three images in Figure 7, the presence of colloidal silver seems to cause an increase in the density of blisters that develop following the exposure of the coatings to the aggressive environment of the salt spray chamber. Furthermore, this phenomenon is even more marked after increasing the amount of silver present in the coatings. Referring to the standard [68], the three series of samples have blisters of size 1–3. However, the density of the blisters increases from grade 3 of sample A, to grades 4 and 5 of samples A1 and A2, respectively. Consequently, silver seems to favor the adsorption of water into the cataphoretic coating, as it represents a point of discontinuity in the acrylic matrix. Figure 8, acquired with the optical stereomicroscope, is exemplar of the high blister density exhibited by sample A2 at the end of the test. The polarizing filter of the microscope made it possible to highlight the morphology of the blisters, which in some cases exceed 2000 µm in size.

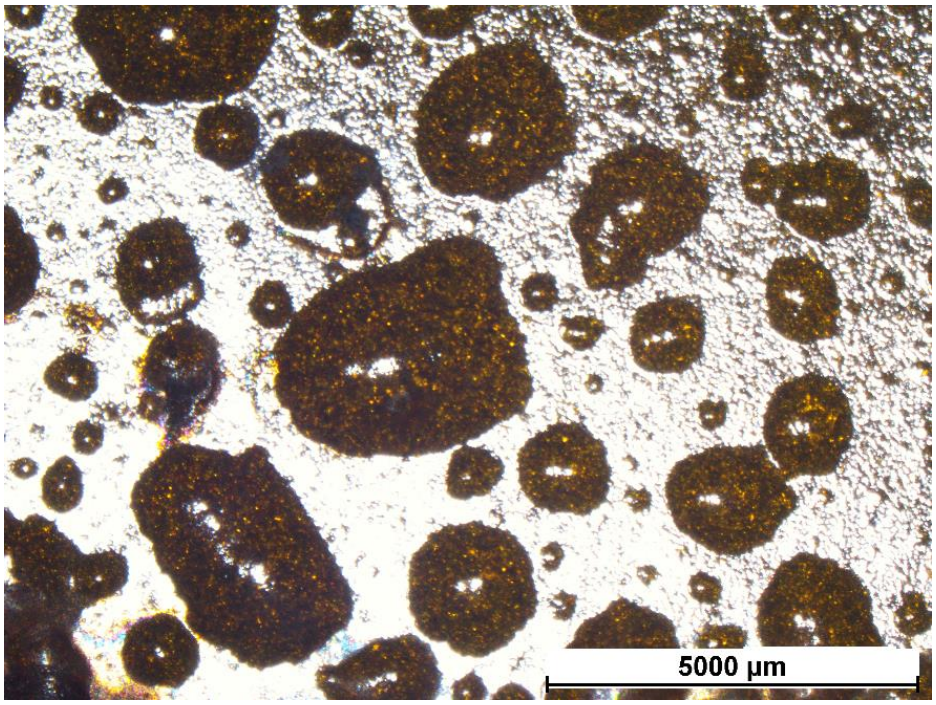


**Figure 8.** Detail of the blisters in sample A2 observed with the optical stereomicroscope at the end of the test.

Therefore, although silver does not introduce apparent defects in the cataphoretic layer, it influences the behavior of the coating for long exposures in aggressive environments. The difference between the results expressed by sample A and sample A1 is almost negligible, while the greater quantity of silver present in the coating A2 seems to play a key role in the durability of the acrylic matrix. To better study the protective characteristics of the three types of coatings evaluating the contribution of silver, the samples were subjected to Electrochemical Impedance Spectroscopy (EIS) measurements.

### *3.3. Electrochemical Impedance Spectroscopy Measurements*

The EIS measurements are widely employed for the estimation of the protective feature of organic coatings, as this technique is able to provide useful details about the corrosion resistance properties of the layer, such as its defectiveness or degree of adhesion [69].

For example, the evolution of the Bode impedance module measured at low frequencies ($10^{-2}$ Hz), defined as $|Z|_{(0.01)}$, can be monitored to get a preliminary quantitative estimation of the degree of protection provided by the coating. The literature defines a minimum value of $|Z|_{(0.01)}$, equal to $10^6$ $\Omega \cdot cm^2$, below which the coating does not ensure certain protective performances [70,71]. Thus, the protective behavior of the three series of coatings was characterized monitoring the evolution over time of their impedance module $|Z|_{(0.01)}$ over time. Figure 9 shows the variation of the parameter $|Z|_{(0.01)}$ during the exposure of 500 h of the samples to the EIS test solution.

The three coatings exhibit different behaviors during the experiment. Sample A reveals a relatively high initial value of $|Z|_{(0.01)}$, which drops, however, by an order of magnitude during the first 4 h of exposure to the test solution. Subsequently, a continuous decrease is observed, with slower speed, until reaching a plateau towards the 340 h of testing. The value of this plateau is very close to the limit of $10^6$ $\Omega \cdot cm^2$, suggesting that the acrylic matrix no longer provides the right protective guarantees.

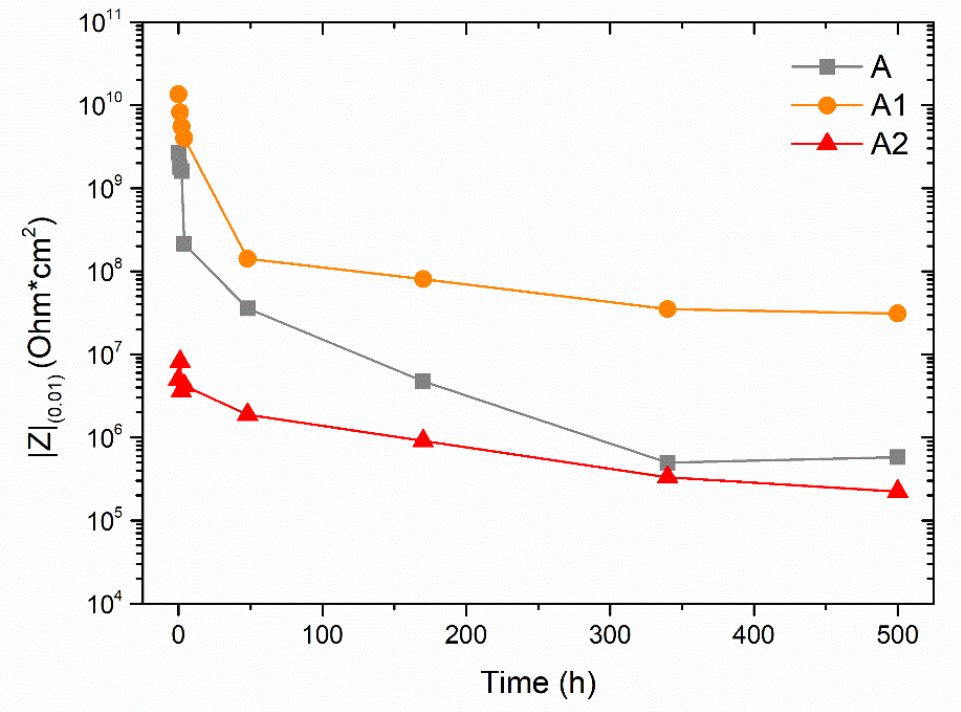


**Figure 9.** Bode impedance modulus $|Z|_{(0.01)}$ evolution with time.

Similarly, sample A1 also shows a sudden decrease in the value of $|Z|_{(0.01)}$ during the first hours of testing. However, the curve quickly settles on high values, equal to about $10^8$ Ω·cm$^2$, keeping this plateau almost unchanged until the end of the test. The improvement of the protective performance of organic coatings by adding silver has already been observed in the literature, under certain conditions [72,73]. This phenomenon can be associated with a decrease in the intrinsic porosity of the acrylic matrix in the presence of limited quantities of silver. By acting as a very low permeability filler, silver is able to reduce the overall porosity of the composite coating. Consequently, the reduced permeability of the coating translates into greater protective performances, expressed by higher values of the impedance module $|Z|_{(0.01)}$.

However, as already observed during exposure in salt spray chamber, too high quantities of silver introduce structural changes in the matrix, increasing its permeability [74]. This phenomenon affects the result of the impedance measurements of sample A2: the trend of $|Z|_{(0.01)}$ immediately starts from lower values than the other two samples, A and A1. In this case, by increasing the permeability of the acrylic matrix, silver reduces its protective properties right away. Throughout the test, sample A2 always shows lower performance than coating A, of the pure acrylic matrix. Having reached 500 h of exposure, $|Z|_{(0.01)}$ comes dangerously close to values of $10^5$ Ω·cm$^2$, evidencing poor protective performance. These results are in agreement with the salt spray test, confirming the criticalities found in the composite coating A2 containing high amount of silver.

The three series of samples showed a strong decrease in $|Z|_{(0.01)}$ mainly during the first 48 h of exposure to the test solution. Indeed, the first hours of immersion are the most significant, as typically the organic coatings undergo solution absorption phenomena. To better analyze the behavior of the three samples and explain the results exhibited in Figure 9, the evolution of the Nyquist diagrams during the first 48 h of the test is displayed in Figure 10. The three images present a box with a focus on low values of $Z'$ and $-Z''$, to highlight the details of the diagrams acquired after 4 h and 48 h of immersion in the test solution.

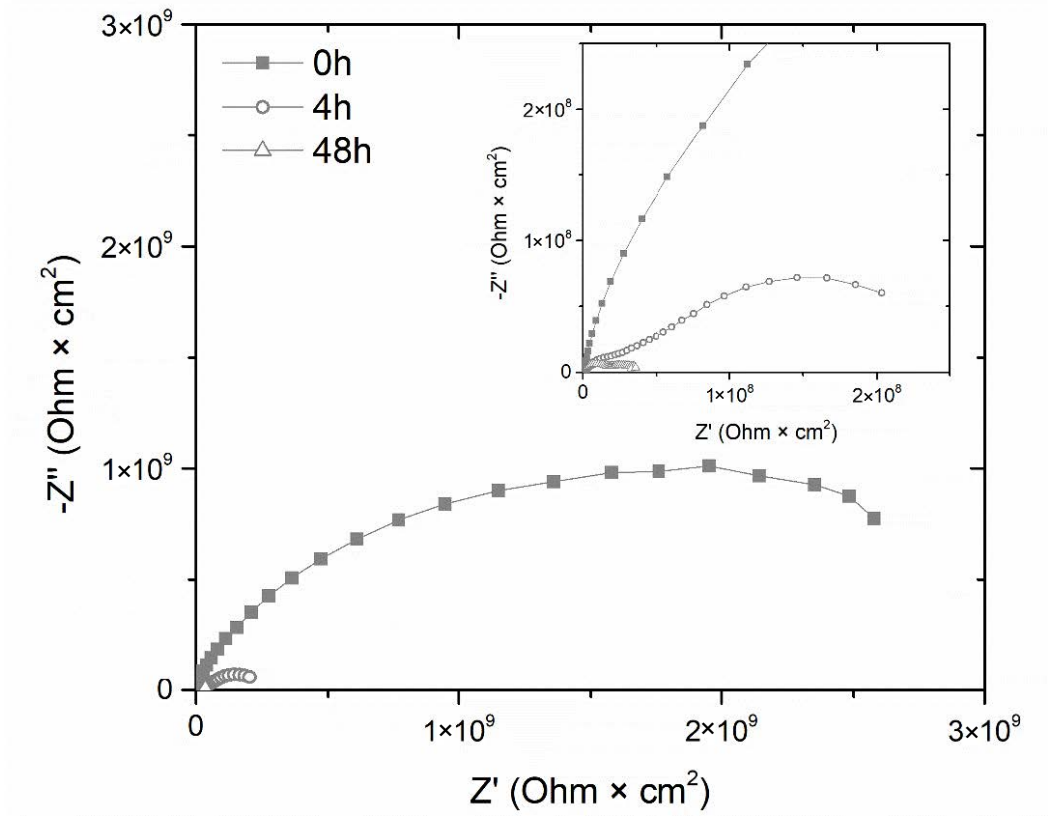


(**a**)

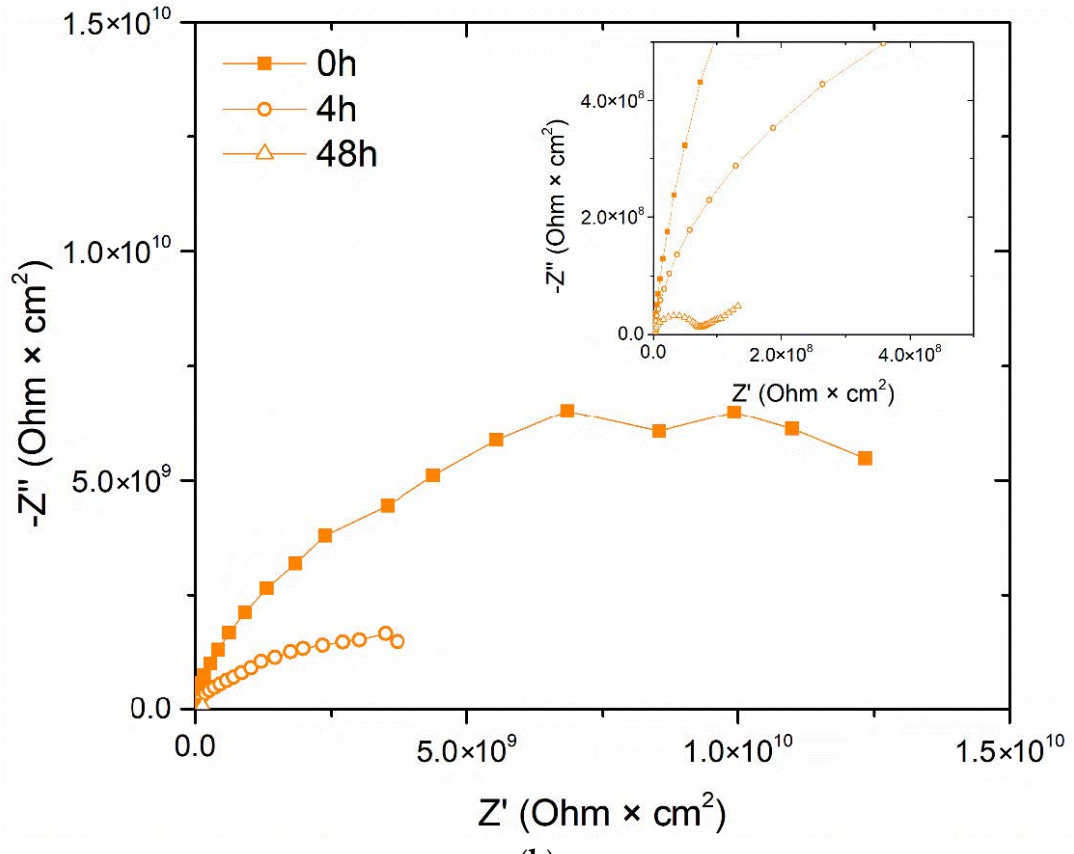


(**b**)

**Figure 10.** *Cont.*

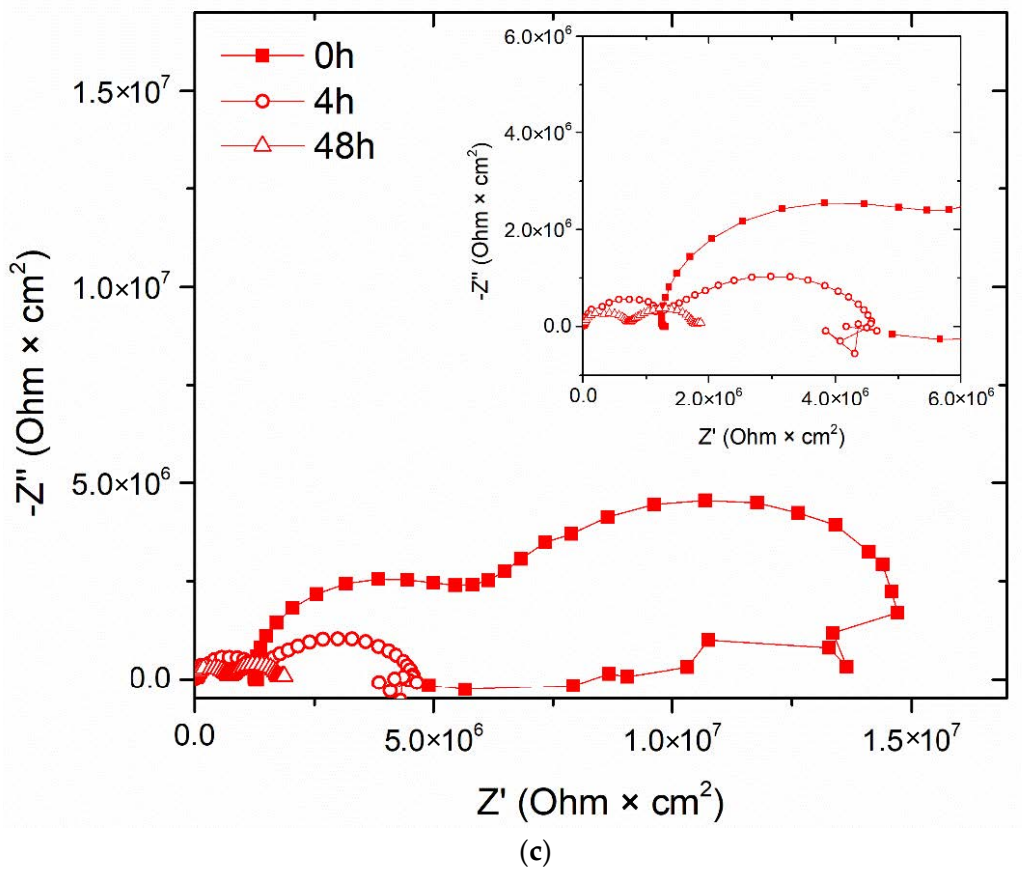


**Figure 10.** Nyquist diagram evolution during the first 48 h of test of the samples A (**a**), A1 (**b**), and A2 (**c**), respectively.

The Nyquist diagrams of sample A (Figure 10a) reveal a rapid decrease in the protective performance of the coating, as both the resistive and capacitive contributions of the acrylic layer are reduced over time. The diagrams represent two-time constants, which are more and more evident as the exposure to the test solution proceeds. The presence of two-time constants indicates the occurrence of corrosion phenomena: the time constant at low frequencies represents, in fact, the dissipative phenomena that occur at the coating-substrate interface, as a consequence of the rapid absorption of the solution. Thus, the acrylic matrix is confirmed to possess intrinsic poor protective features.

The diagrams in Figure 10b (sample A1) exhibit a similar trend, even if the two-time constants can only be appreciated after 48 h of measurements. The dissipation phenomena below the coating seem to be postponed over time, suggesting the barrier effect introduced by silver, which acts as a filler for the porosity of the acrylic matrix. This phenomenon translates into a better protective performance of sample A1 throughout the test.

Finally, the Nyquist diagrams of sample A2 (Figure 10c) provide the most significant information. The two-time constants are already evident in the diagram acquired at the start of the test, which shows two distinct semicircles. However, the second semicircle, representative of the dissipative phenomena due to the composite coating, tends to close in on itself, with the curve returning to lower Z′ values. This is a typical behavior of systems in continuous evolution during the measurement itself: it represents the tendency of the composite coating to absorb a considerable amount of solution, so as to make the data acquisition pretty unstable. Consequently, the impedance values, already low at the start of the measurements, tend to decrease quickly until they reach and exceed the safety threshold of $10^6$ Ω·cm$^2$, as shown in Figure 9.

The behavior of the three series of samples is well represented by the images in Figure 11, representative of the surfaces subjected to the EIS measurements after 500 h

of immersion in the test solution. The surfaces of the three samples exhibit some small dark corrosion products, but still differ in the density of blisters developed during the experiment. More than half of the surface of the coating A reveals the presence of blisters of different sizes. The addition of 0.05 wt.% of colloidal silver results in an improvement in the durability of the acrylic matrix, as the development of blisters is limited. Finally, the poor results of the EIS measurements relating to sample A2 can be appreciated from the appearance of the coating, whose surface at the end of the test is completely covered with blisters.

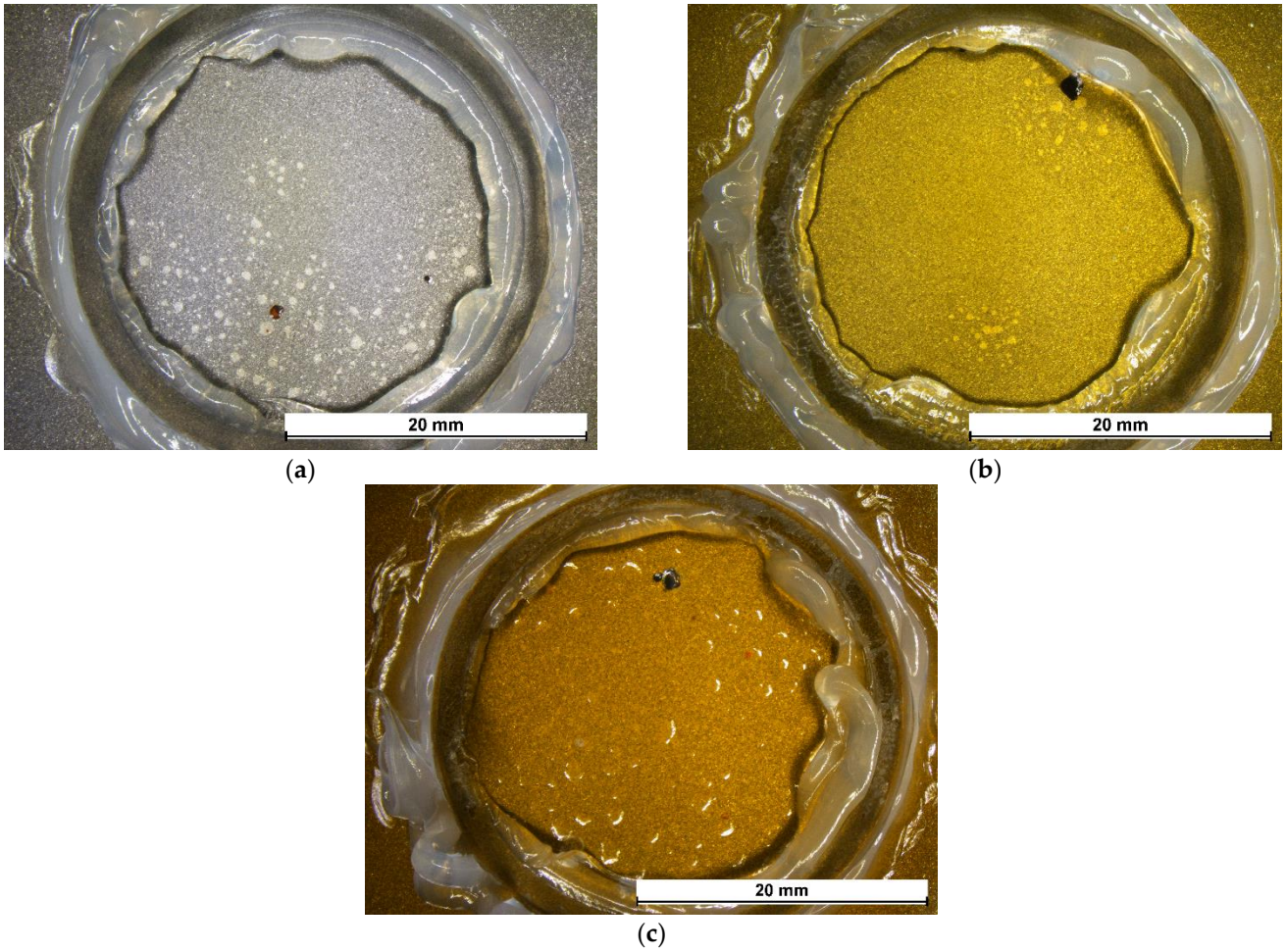


(**a**) (**b**) (**c**)

**Figure 11.** Surface of sample A (**a**), A1 (**b**) and A2 (**c**), after 500 h of immersion in test solution.

Therefore, the simple observation of the surfaces of the three coatings provides realistic information on their protective performance, in agreement with the results of specific techniques such as the electrochemical impedance spectroscopy measurements.

As both the test of exposure in salt spray chamber and the EIS measurements exhibit comparable results, the positive contribution introduced by small quantities of colloidal silver has been confirmed. However, the addition of Ag can take on negative connotations if a limit concentration is exceeded, reducing the protective performance of the acrylic matrix.

### *3.4. Exposure to UV-B Radiation*

Ultraviolet radiation can affect the aesthetic features of organic coatings, causing their chemical degradation. Thus, UV-B exposure is a procedure widely employed for the assessment of the durability of organic coatings, which must ensure a long outdoor service life [75,76].

While the limited effect of solar radiation on acrylic resins is well known [77,78], recent studies highlighted the degradation phenomena that silver can undergo when exposed to UV light, in terms of retention, dissolution, and oxidative aging [79,80]. The extent of these phenomena can also be exacerbated due to the combination with high temperatures [81]. Therefore, the samples were exposed for 500 h to UV-B radiation at 50 °C, evaluating the change in aesthetic features of the cataphoretic coatings.

Figure 12 shows the total color variation, ΔE, every 100 h of UV-B light exposure. According to the ASTM E308 (2018) standard [82], ΔE is calculated as follows:

$$\Delta E = [(\Delta L^*)^2 + (\Delta a^*)^2 + (\Delta b^*)^2]^{1/2} \quad (1)$$

where the colorimetric coordinates L*, a* and b* represents the lightness (0 for black and 100 for white objects), the red–green coordinate (positive values are red, negative values are green), and the yellow–blue coordinate (yellow for positive values, blue for negative values and 0 as neutral parameter), respectively.

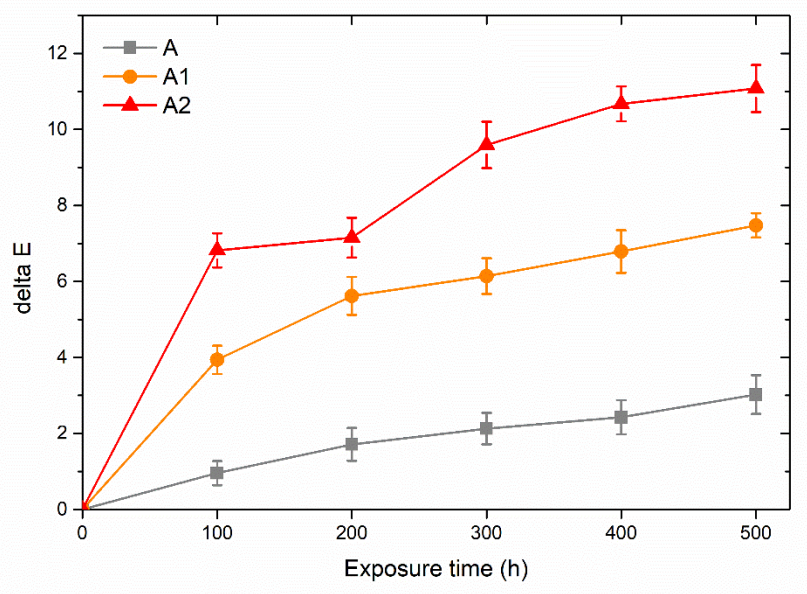


**Figure 12.** Total color variation during UV-B exposure.

ΔE = 1 is considered the threshold value for which the color difference is imperceptible to the human eye [83]. Consequently, the coating A exhibited a limited change in appearance. The color of the acrylic matrix varied constantly during the test; however, it always remained very close to the initial coordinates. Indeed, after 500 h of exposure to the UV-B light, coating A revealed a value of ΔE approximately equal to three, confirming the good durability of the acrylic matrix against solar radiation.

Otherwise, the two silver-containing coatings underwent a noticeable color change. Silver proves to suffer particularly from exposure to UV-B rays, as sample A1 and sample A2 exhibited a sudden and not negligible change in color. After only 100 h of exposure, the color change reaches values over half of the total ΔE observed during the entire test. The greater the quantity of silver contained in the acrylic matrix, the greater the variation in the aesthetic features of the coating, but also the more intense the degradation due to the exposure to UV-B radiation.

Figure 13 compares the evolution of the appearance of the three coatings during the UV-B exposure test. While the degradation of coating A cannot be appreciated, the human eye easily recognizes the tendency of the coatings containing silver to become darker.

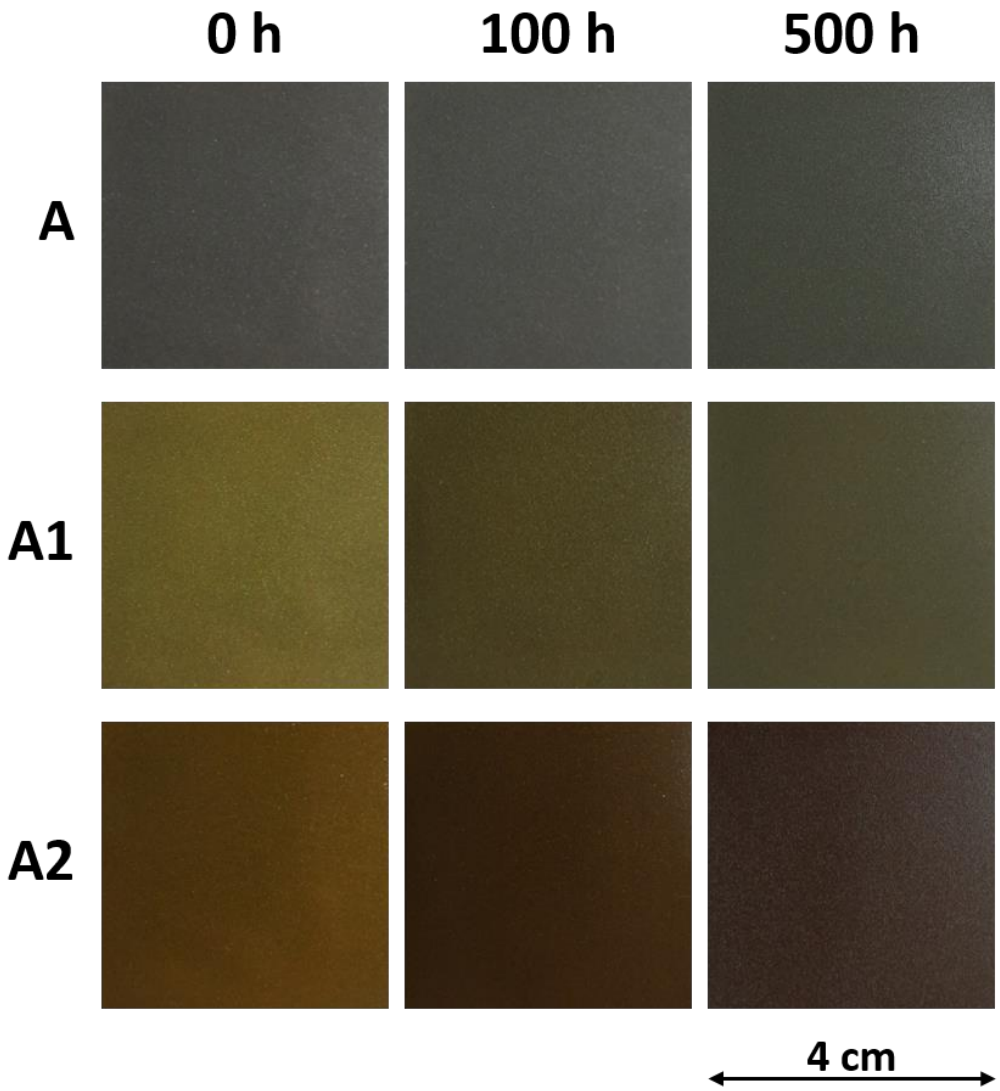


**Figure 13.** Evolution of the appearance of the coatings during the exposure to UV-B radiation.

However, this phenomenon is due to the variation of the values of the coordinates a* and b*, as shown in the Table 3, rather than linked to a decrease in the brightness (L*) of the coating.

**Table 3.** Evolution of the colorimetric coordinates of the samples during the exposure to UV-B radiation.

| | A | | | A1 | | | A2 | | |
|---|---|---|---|---|---|---|---|---|---|
| **Time [h]** | **L*** | **a*** | **b*** | **L*** | **a*** | **b*** | **L*** | **a*** | **b*** |
| 0 | 48.26 | 0.11 | 2.26 | 43.61 | 0.77 | 17.96 | 38.01 | 6.3 | 19.32 |
| 100 | 47.43 | −0.18 | 2.64 | 42.48 | 2.95 | 14.88 | 34.97 | 10.23 | 14.65 |
| 200 | 47.18 | −0.44 | 3.47 | 41.36 | 2.76 | 13.21 | 34.65 | 9.2 | 13.71 |
| 300 | 47.02 | −0.47 | 3.89 | 41.06 | 2.68 | 12.71 | 33.41 | 9.83 | 11.68 |
| 400 | 47.37 | −0.47 | 4.44 | 41.06 | 2.31 | 11.86 | 34.4 | 7.59 | 9.36 |
| 500 | 46.79 | −0.4 | 4.85 | 40.95 | 2.2 | 11.12 | 35.89 | 6.13 | 8.45 |

Before exposure to UV-B radiation, the addition of silver in the acrylic matrix caused a decrease in the brightness of the coating (lower L* values) and an increase in the coordinates a* and b*, representative of shades tending to red and yellow, respectively. Subsequently,

the parameter b*, even more than the coordinate a*, varies towards lower values, decreasing the yellow shade of the composite coating. During the whole test, sample A1 and sample A2 showed total Δb* of approximately 7 points and 11 points, respectively. Definitively, this variation in the values of the color coordinates, with consequent darkening of the appearance of the coating, is mainly due to the oxidation phenomena [84] that silver undergoes during UV-B exposure.

The aesthetic variation of the silver-containing coatings is also closely linked to a morphological degradation of the composite layers. Figure 14 reveals the surface of sample A1 and sample A2 observed with the optical microscope at the end of the experiment, after 500 h of exposure to UV-B radiation. Both coatings show the development of some blisters within the acrylic matrix. This phenomenon is intensified in sample A2, suggesting that it has been caused by the presence of silver. Dissolution of silver, due to UV exposure, is supposed to have created these voids and blisters in the acrylic matrix. In addition to a purely aesthetic aspect, this phenomenon represents a critical defect in the coating, as the permeability of the acrylic matrix is further exasperated, compromising its durability. It must be considered that the exposure to UV-B radiation represents a particularly aggressive test, not fully simulating the exposure to sunlight, in terms of frequency and intensity of the radiation. However, the degradation of silver inevitably also leads to a decrease in the protective performance of the cataphoretic coating, suggesting the application of this type of coating only on products designed for indoor applications.

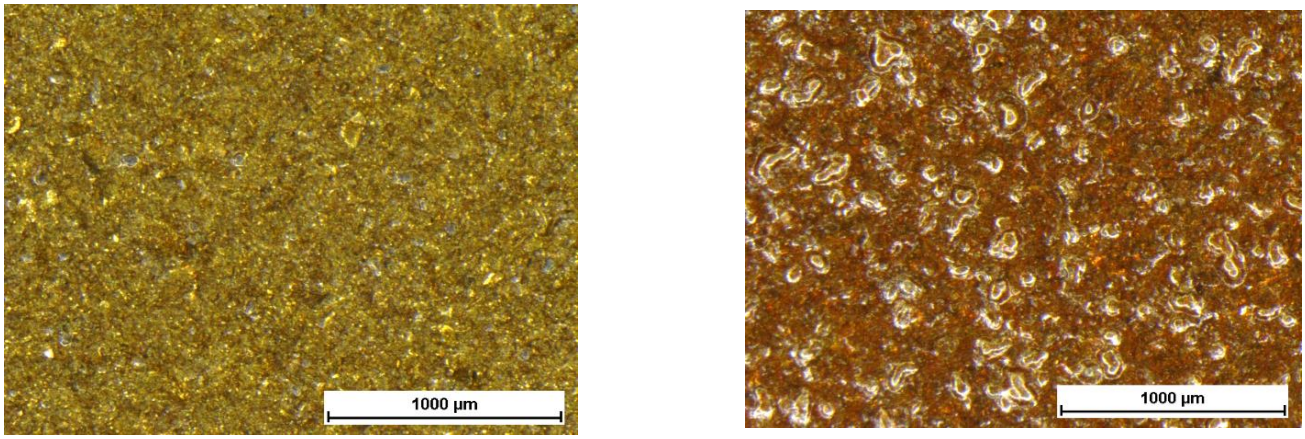


(**a**) (**b**)

**Figure 14.** Detail of the blisters in samples A1 (**a**) and A2 (**b**), observed with the optical stereomicroscope after 500 h of exposure to UV-B radiation.

The silver concentration detected by EDXS analyses in sample A1 and sample A2, equal to 1.4 wt.% and about 3 wt.%, respectively, provides high guarantees on the antibacterial performance of both types of coatings. In fact, other works have confirmed the high antibacterial functionality of silver in low concentrations, even lower than those evidenced by the two composite coatings [42,48]. While coating A2 possesses high defects, with consequent poor durability performance, the quantity of silver present in coating A1 allows both to offer guarantees from the point of view of antibacterial properties, and to increase the protective performance of the acrylic matrix. Consequently, coating A1 can be used in various application fields where good durability is required, in combination with effective antibacterial features.

## 4. Conclusions

The effect of the addition of colloidal silver on the durability of the cataphoretic coating has been evaluated in this work. The introduction of colloidal silver in the cataphoretic bath caused a significant change in the aesthetic features of the coating, whose color tended towards yellow and orange, the tones of which strongly depended on the concentration

of the silver-based filler. Colloidal silver, completely soluble in water, did not introduce defects in the coating and did not influence the electrodeposition process. However, the reaction with the acrylic resin caused limited agglomerations of the silver ions to form discontinuities in the acrylic matrix.

These discontinuities can favor an increase in the permeability of the acrylic matrix, reducing its protective performance. The exposure of the samples in the salt spray chamber highlighted the high absorption of the test solution by the coating containing a high amount of silver. The presence of silver did not directly influence the adhesion of the coating, but favored the water uptake in the acrylic matrix, with consequent development of the high blister density and corrosion products at the interface with the metal substrate.

This phenomenon was confirmed by the electrochemical impedance spectroscopy measurements, which demonstrated a sudden absorption of the test solution by the coating A2, which, in turn, exhibited a decrease in the protective performance of the acrylic matrix. However, the limited amount of silver present in sample A1 resulted in an improvement in the protective behavior of the cataphoretic coating, as the colloidal silver acted as a filler for the porosity of the acrylic matrix. As a matter of fact, after 500 h of exposure to the test solution, sample A1 exhibited a $|Z|(0.01)$ value equal to 108 $\Omega \cdot cm^2$, two orders of magnitude higher than the pure acrylic matrix of coating A.

Finally, the exposure of the samples to UV-B radiation confirmed the high reactivity of silver-based fillers when subjected to sunlight. The rapid oxidation of silver caused a darkening of the appearance of the coating, as evidenced by the colorimetric measurements, but is also visually appreciable. At the same time, the dissolution of silver led to the development of blisters in the acrylic matrix, especially in sample A2, which was produced with a high amount of silver.

Ultimately, this work highlights the merits and criticalities in the use of colloidal silver as a filler in acrylic cataphoretic baths. High concentrations of colloidal silver can introduce discontinuities in the acrylic matrix, reducing its durability, but in certain quantities the silver is also able to improve the protective performance of the composite coating. From an aesthetic point of view, colloidal silver also acts as a particular pigment, the effect of which, however, is significantly influenced by the oxidative and dissolutive phenomena that occur due to exposure to solar radiation.

Thus, colloidal silver represents a suitable filler in cataphoretic processes, but needs a targeted control on the adequate amount, in order to avoid being negative for the durability of the coating itself.

**Author Contributions:** Conceptualization, M.C. and S.R.; methodology, M.C. and S.R.; investigation, M.C.; data curation, M.C. and S.R.; writing—original draft preparation, M.C.; writing—review and editing, M.C. and S.R.; supervision, S.R. All authors have read and agreed to the published version of the manuscript.

**Funding:** This research was funded by the RIVID project granted by the University of Trento in 2020 in the context of the "Covid19" call awarded to S.R. (coordinator).

**Institutional Review Board Statement:** Not applicable.

**Informed Consent Statement:** Not applicable.

**Data Availability Statement:** The data presented in this study are available on request from the corresponding author. The data are not publicly available due to the absence of an institutional repository.

**Acknowledgments:** The authors greatly acknowledge the contributions of Gianluca Gazzola and Marzio Marchesi (Arsonsisi, Lainate MI, Italy) regarding the paint bath supply.

**Conflicts of Interest:** The authors declare no conflict of interest.

## References


1. Abdellah, A.; Fabel, B.; Lugli, P.; Scarpa, G. Spray deposition of organic semiconducting thin-films: Towards the fabrication of arbitrary shaped organic electronic devices. *Org. Electron.* **2010**, *11*, 1031–1038. [CrossRef]
2. Aleksandrova, M.; Andreev, S.; Kolev, G. Spray deposition of organic electroluminescent coatings for application in flexible light emitting devices. *Cogent Eng.* **2015**, *2*, 1014248. [CrossRef]
3. Girotto, C.; Rand, B.P.; Genoe, J.; Heremans, P. Exploring spray coating as a deposition technique for the fabrication of solution-processed solar cells. *Sol. Energy Mater. Sol. Cells* **2009**, *93*, 454–458. [CrossRef]
4. Sparks, B.J.; Hoff, E.F.T.; Xiong, L.; Goetz, J.T.; Patton, D.L. Superhydrophobic Hybrid inorganic–organic thiol-ene surfaces fabricated via spray-deposition and photopolymerization. *ACS Appl. Mater. Interfaces* **2013**, *5*, 1811–1817. [CrossRef] [PubMed]
5. Ramdé, T.; Ecco, L.G.; Rossi, S. Visual appearance durability as function of natural and accelerated ageing of electrophoretic styrene-acrylic coatings: Influence of yellow pigment concentration. *Prog. Org. Coat.* **2017**, *103*, 23–32. [CrossRef]
6. Deflorian, F.; Rossi, S.; Prosseda, S. Improvement of corrosion protection system for aluminium body bus used in public transportation. *Mater. Des.* **2006**, *27*, 758–769. [CrossRef]
7. Rossi, S.; Calovi, M.; Fedel, M. Corrosion protection of aluminum foams by cataphoretic deposition of organic coatings. *Prog. Org. Coat.* **2017**, *109*, 144–151. [CrossRef]
8. Karacal, P.N.; Elginoz, N.; Babuna, F.G. Environmental burdens of cataphoresis process. *Desalin. W. Treat.* **2019**, *172*, 301–308. [CrossRef]
9. Almeida, E.; Alves, I.; Brites, C.; Fedrizzi, L. Cataphoretic and autophoretic automotive primers: A comparative study. *Prog. Org. Coat.* **2003**, *46*, 8–20. [CrossRef]
10. Skotnicki, W.; Jędrzejczyk, D. The comparative analysis of the coatings deposited on the automotive parts by the cataphoresis method. *Materials* **2021**, *14*, 6155. [CrossRef]
11. Youssouf, H.; Azzouzi, S.R.; Reklaoui, K. Control of the "Cataphoresis" Process by Artificial Intelligence. In Proceedings of the Advances in Intelligent Systems and Computing, Marrakech, Morocco, 8–11 July 2019; pp. 169–188.
12. Hylák, K.; Matuška, Z.; Drašnar, P.; Kudláček, J.; Horník, J. Development of equipment for mass cataphoresis painting. *Mater. Sci. Forum* **2019**, *952*, 92–98. [CrossRef]
13. Benato, A. Improving the efficiency of a cataphoresis oven with a cogenerative organic Rankine cycle unit. *Therm. Sci. Eng. Prog.* **2018**, *5*, 182–194. [CrossRef]
14. García, S.; Rodríguez, M.T.; Izquierdo, R.; Suay, J. Evaluation of cure temperature effects in cataphoretic automotive primers by electrochemical techniques. *Prog. Org. Coat.* **2007**, *60*, 303–311. [CrossRef]
15. García, S.; Suay, J. Optimization of deposition voltage of cataphoretic automotive primers assessed by EIS and AC/DC/AC. *Prog. Org. Coat.* **2009**, *66*, 306–313. [CrossRef]
16. Araújo, E.; Rodrigues, M.A.; Viana, A.; Viana, R. The influence of glycerol as an additive in Zinc-Manganese alloy coatings formed by electrodeposition. *Acta Sci. Technol.* **2019**, *41*, 41103. [CrossRef]
17. Bučko, M.; Mišković-Stanković, V.; Rogan, J.; Bajat, J.B. The protective properties of epoxy coating electrodeposited on Zn-Mn alloy substrate. *Prog. Org. Coat.* **2015**, *79*, 8–16. [CrossRef]
18. Szklarska, M.; Łosiewicz, B.; Dercz, G.; Maszybrocka, J.; Rams-Baron, M.; Stach, S. Electrophoretic deposition of chitosan coatings on the Ti15Mo biomedical alloy from a citric acid solution. *RSC Adv.* **2020**, *10*, 13386–13393. [CrossRef]
19. Zanella, C.; Pedrotti, A.; Fedel, M.; Deflorian, F. Influence of the electrochemical behavior of metal substrates on the properties of cataphoretic clearcoat. *Prog. Org. Coat.* **2014**, *77*, 1987–1992. [CrossRef]
20. Živković, L.S.; Bajat, J.B.; Popić, J.P.; Jegdić, B.V.; Stevanović, S.; Mišković-Stanković, V.B. Protective properties of cataphoretic epoxy coating on aluminium alloy AA6060 modified with electrodeposited Ce-based coatings: Effect of post-treatment. *Prog. Org. Coat.* **2015**, *79*, 43–52. [CrossRef]
21. Romano, A.P.; Olivier, M.G.; Nazarov, A.; Thierry, D. Influence of crosslinking density of a cataphoretic coating on initiation and propagation of filiform corrosion of AA6016. *Prog. Org. Coat.* **2009**, *66*, 173–182. [CrossRef]
22. Reichinger, M.; Bremser, W.; Dornbusch, M. Interface and volume transport on technical cataphoretic painting: A comparison of steel, hot-dip galvanised steel and aluminium alloy. *Electrochim. Acta* **2017**, *231*, 135–152. [CrossRef]
23. Romano, A.-P.; Fedel, M.; Deflorian, F.; Olivier, M.G. Silane sol–gel film as pretreatment for improvement of barrier properties and filiform corrosion resistance of 6016 aluminium alloy covered by cataphoretic coating. *Prog. Org. Coat.* **2011**, *72*, 695–702. [CrossRef]
24. Fedel, M. Effect of sol–gel layers obtained from GLYMO/MTES mixtures on the delamination of a cataphoretic paint on AA1050. *J. Coat. Technol. Res.* **2017**, *14*, 425–435. [CrossRef]
25. Zivkovic, L.S.; Jegdjc, B.V.; Andric, V.; Rhee, K.Y.; Bajat, J.B.; Miakovjc Stankovic, V. The effect of ceria and zirconia nanoparticles on the corrosion behaviour of cataphoretic epoxy coatings on AA6060 alloy. *Prog. Org. Coat.* **2019**, *136*, 105219. [CrossRef]
26. Jegdić, B.V.; Živković, L.S.; Popić, J.P.; Rogan, J.; Bajat, J.B.; Mišković-Stanković, V.B. Corrosion stability of cerium-doped cataphoretic epoxy coatings on AA6060 alloy. *Mater. Corros.* **2016**, *67*, 1173–1184. [CrossRef]
27. Rossi, S.; Calovi, M. Addition of graphene oxide plates in cataphoretic deposited organic coatings. *Prog. Org. Coat.* **2018**, *125*, 40–47. [CrossRef]
28. Calovi, M.; Dirè, S.; Ceccato, R.; Deflorian, F.; Rossi, S. Corrosion protection properties of functionalised graphene–acrylate coatings produced via cataphoretic deposition. *Prog. Org. Coat.* **2019**, *136*, 105261. [CrossRef]

29. Calovi, M.; Rossi, S.; Deflorian, F.; Dirè, S.; Ceccato, R. Effect of functionalized graphene oxide concentration on the corrosion resistance properties provided by cataphoretic acrylic coatings. *Mater. Chem. Phys.* **2019**, *239*, 121984. [CrossRef]
30. Calovi, M.; Rossi, S.; Deflorian, F.; Dirè, S.; Ceccato, R.; Guo, X.; Frankel, G.S. Effects of graphene-based fillers on cathodic delamination and abrasion resistance of cataphoretic organic coatings. *Coatings* **2020**, *10*, 602. [CrossRef]
31. Calovi, M.; Russo, F.; Rossi, S. Synergic behavior of graphene-based filler and thermochromic pigments in cataphoretic coatings. *Prog. Org. Coat.* **2021**, *150*, 105978. [CrossRef]
32. Calovi, M.; Russo, F.; Rossi, S. Esthetic performance of thermochromic pigments in cataphoretic and sprayed coatings for outdoor applications. *J. Appl. Polym. Sci.* **2021**, *138*, 50622. [CrossRef]
33. El-Faham, A.; Atta, A.M.; Osman, S.M.; Ezzat, A.O.; El-saeed, A.M.; Al Othman, Z.A.; Al-Lohedan, H.A. Silver-embedded epoxy nanocomposites as organic coatings for steel. *Prog. Org. Coat.* **2018**, *123*, 209–222. [CrossRef]
34. Giraldo Mejía, H.F.; Herrera Seitz, K.; Valdés, M.; Uheida, A.; Procaccini, R.A.; Pellice, S.A. Antibacterial performance of hybrid nanocomposite coatings containing clay and silver nanoparticles. *Colloids Surf. A Physicochem. Eng. Asp.* **2021**, *628*, 127354. [CrossRef]
35. Rozilah, A.; Aiza Jaafar, C.N.; Sapuan, S.M.; Zainol, I.; Ilyas, R.A. The effects of silver nanoparticles compositions on the mechanical, physiochemical, antibacterial, and morphology properties of sugar palm starch biocomposites for antibacterial coating. *Polymers* **2020**, *12*, 2605. [CrossRef]
36. Rai, N.K.; Ashok, A.; Akondi, B.R. Consequences of chemical impact of disinfectants: Safe preventive measures against COVID-19. *Crit. Rev. Toxicol.* **2020**, *50*, 513–520. [CrossRef] [PubMed]
37. Russell, A.; Hugo, W. 7 antimicrobial activity and action of silver. *Prog. Med. Chem.* **1994**, *31*, 351–370. [PubMed]
38. Karunagaran, V.; Rajendran, K.; Sen, S. Antimicrobial activity of biosynthesized silver oxide nanoparticles. *J. Pure Appl. Microbiol.* **2014**, *4*, 3263–3268.
39. Swathy, J.R.; Sankar, M.U.; Chaudhary, A.; Aigal, S.; Anshup; Pradeep, T. Antimicrobial silver: An unprecedented anion effect. *Sci. Rep.* **2014**, *4*, 7161. [CrossRef]
40. Schneider, G. Antimicrobial silver nanoparticles–Regulatory situation in the European Union. *Mater. Today Proc.* **2017**, *4*, S200–S207. [CrossRef]
41. Yin, I.; Zhang, J.; Zhao, I.; Mei, M.L.; Li, Q.; Chu, C.-H. The Antibacterial mechanism of silver nanoparticles and its application in dentistry. *Int. J. Nanomed.* **2020**, *15*, 2555–2562. [CrossRef]
42. Vimbela, G.; Sang, N.; Fraze, C.; Yang, L.; Stout, D. Antibacterial properties and toxicity from metallic nanomaterials [Corrigendum]. *Int. J. Nanomed.* **2018**, *13*, 6497–6498. [CrossRef] [PubMed]
43. Noronha, V.T.; Paula, A.J.; Durán, G.; Galembeck, A.; Cogo-Müller, K.; Franz-Montan, M.; Duran, N. Silver nanoparticles in dentistry. *Dent. Mater.* **2017**, *33*, 1110–1126. [CrossRef] [PubMed]
44. Gonzalo-Juan, I.; Xie, F.; Becker, M.; Tulyaganov, D.U.; Ionescu, E.; Lauterbach, S.; De Angelis Rigotti, F.; Fischer, A.; Riedel, R. Synthesis of silver modified bioactive glassy materials with antibacterial properties via facile and low-temperature route. *Materials* **2020**, *13*, 5115. [CrossRef] [PubMed]
45. da Silva, L.C.A.; Neto, F.G.; Pimentel, S.S.C.; Palácios, R.d.S.; Sato, F.; Retamiro, K.M.; Fernandes, N.S.; Nakamura, C.V.; Pedrochi, F.; Steimacher, A. The role of Ag2O on antibacterial and bioactive properties of borate glasses. *J. Non-Cryst. Sol.* **2021**, *554*, 120611. [CrossRef]
46. Dharmaraj, D.; Krishnamoorthy, M.; Rajendran, K.; Karuppiah, K.; Annamalai, J.; Durairaj, K.R.; Santhiyagu, P.; Ethiraj, K. Antibacterial and cytotoxicity activities of biosynthesized silver oxide (Ag2O) nanoparticles using Bacillus paramycoides. *J. Drug Deliv. Sci. Technol.* **2021**, *61*, 102111. [CrossRef]
47. Agbe, H.; Sarkar, D.K.; Chen, X.G. Electrochemically synthesized silver phosphate coating on anodized aluminum with superior antibacterial properties. *Surf. Coat. Technol.* **2021**, *428*, 127892. [CrossRef]
48. Calovi, M.; Furlan, B.; Coroneo, V.; Massidda, O.; Rossi, S. Facile route to effective antimicrobial aluminum oxide layer realized by co-deposition with silver nitrate. *Coatings* **2022**, *12*, 28. [CrossRef]
49. Dehghan, F.; Mardanpour, H.; Kamali, S.; Alirezaei, S. Synthesis and antibacterial properties of novel $Al_2O_3$-Ag anodised composite coating. *Mater. Technol.* **2021**, *36*, 721–730. [CrossRef]
50. Zhang, L.; Li, B.; Zhang, X.; Wang, D.; Zhou, L.; Li, H.; Liang, C.; Liu, S.; Wang, H. Biological and antibacterial properties of $TiO_2$ coatings containing Ca/P/Ag by one-step and two-step methods. *Biomed. Microdevices* **2020**, *22*, 24. [CrossRef]
51. Chen, D.; Li, Y.; He, H.; Li, W.; Zeng, R.; Wang, X. Covalent incorporation of Ag nanoparticles into $TiO_2$ nanotubes on $Ti_6Al_4V$ by molecular grafting for enhancing antibacterial effect. *Surf. Coat. Technol.* **2021**, *426*, 127773. [CrossRef]
52. Makowski, T.; Svyntkivska, M.; Piorkowska, E.; Mizerska, U.; Fortuniak, W.; Kowalczyk, D.; Brzezinski, S.; Kregiel, D. Antibacterial electroconductive composite coating of cotton fabric. *Materials* **2022**, *15*, 1072. [CrossRef] [PubMed]
53. Chen, Y.; Li, W.; Wang, W.; Zhao, Y.; Chen, M. Microstructure, corrosion resistance, and antibacterial properties of an Ag/Mg-Al layered double hydroxide coating synthesized in situ on biomedical Mg-Zn-Ca alloy. *Ceram. Int.* **2022**, *48*, 4172–4187. [CrossRef]
54. Ganguli, P.; Chaudhuri, S. Nanomaterials in antimicrobial paints and coatings to prevent biodegradation of man-made surfaces: A review. *Mater. Today Proc.* **2020**, *45*, 3769–3777. [CrossRef]
55. Abdullayev, E.; Sakakibara, K.; Okamoto, K.; Wei, W.; Ariga, K.; Lvov, Y. Natural tubule clay template synthesis of silver nanorods for antibacterial composite coating. *ACS Appl. Mater. Interfaces* **2011**, *3*, 4040–4046. [CrossRef] [PubMed]

56. Cheng, L.; Ren, S.; Lu, X. Application of eco-friendlywaterborne polyurethane composite coating incorporated with nano cellulose crystalline and silver nano particles on wood antibacterial board. *Polymers* **2020**, *12*, 407. [CrossRef] [PubMed]
57. Yan, X.; Pan, P. Preparation of silver antibacterial agents with different forms and their effects on the properties of water-based primer on tilia europaea surface. *Coatings* **2021**, *11*, 1066. [CrossRef]
58. Wang, L.; Porto, C.L.; Palumbo, F.; Modic, M.; Cvelbar, U.; Ghobeira, R.; De Geyter, N.; De Vrieze, M.; Serša, G.; Leys, C.; et al. Synthesis of antibacterial composite coating containing nanocapsules in an atmospheric pressure plasma. *Mater. Sci. Eng. C* **2021**, *119*, 111496. [CrossRef]
59. Lateef, A.; Azeez, M.A.; Asafa, T.B.; Yekeen, T.A.; Akinboro, A.; Oladipo, I.C.; Azeez, L.; Ajibade, S.E.; Ojo, S.A.; Gueguim-Kana, E.B.; et al. Biogenic synthesis of silver nanoparticles using a pod extract of Cola nitida: Antibacterial and antioxidant activities and application as a paint additive. *J. Taibah Univ. Sci.* **2016**, *10*, 551–562. [CrossRef]
60. Deya, C.; Bellotti, N. Biosynthesized silver nanoparticles to control fungal infections in indoor environments. *Adv. Nat.Sci. Nanosci. Nanotechnol.* **2017**, *8*, 025005. [CrossRef]
61. Barberia-Roque, L.; Gámez-Espinosa, E.; Viera, M.; Bellotti, N. Assessment of three plant extracts to obtain silver nanoparticles as alternative additives to control biodeterioration of coatings. *Int. Biodeterior. Biodegrad.* **2019**, *141*, 52–61. [CrossRef]
62. Liu, S.; He, J.; Xue, J.; Ding, W. Efficient fabrication of transparent antimicrobial poly(vinyl alcohol) thin films. *J. Nanopart. Res.* **2009**, *11*, 553–560. [CrossRef]
63. Bechtold, M.; Valério, A.; Souza, A.; Oliveira, D.; Franco, C.; Serafim, R.; Guelli Souza, S. Synthesis and application of silver nanoparticles as biocidal agent in polyurethane coating. *J. Coat. Technol. Res.* **2020**, *17*, 613–620. [CrossRef]
64. Asafa, T.; Odediji, R.; Salaudeen, T.; Lateef, A.; Durowoju, M.; Azeez, M.; Yekeen, T.; Oladipo, I.; Irshad, H.M.; Hakeem, A. Physico-mechanical properties of emulsion paint embedded with silver nanoparticles. *Bull. Mater. Sci.* **2021**, *44*, 7. [CrossRef]
65. Ohashi, F.; Shibahara, A. Antibacterial and antifungal properties of clear coating film containing silver–cytokinin complex as a filler. *J. Coat. Technol. Res.* **2020**, *17*, 1619–1623. [CrossRef]
66. *ASTM B117:2011*; Operating Salt Spray (Fog) Apparatus. ASTM: West Conshohocken, PA, USA, 2011; pp. 1–12.
67. *ASTM G154:16*; Standard Practice for Operating Fluorescent Ultraviolet (UV) Lamp Apparatus for Exposure of Nonmetallic Materials. ASTM: West Conshohocken, PA, USA, 2016.
68. *ISO 4628*; Evaluation of Degradation of Coatings. ISO: Geneva, Switzerland, 2012.
69. Deflorian, F.; Rossi, S. An EIS study of ion diffusion through organic coatings. *Electrochim. Acta* **2006**, *51*, 1736–1744. [CrossRef]
70. Amirudin, A.; Thieny, D. Application of electrochemical impedance spectroscopy to study the degradation of polymer-coated metals. *Prog. Org. Coat.* **1995**, *26*, 1–28. [CrossRef]
71. Akbarinezhad, E.; Bahremandi, M.; Faridi, H.; Rezaei, F. Another approach for ranking and evaluating organic paint coatings via electrochemical impedance spectroscopy. *Corros. Sci.* **2009**, *51*, 356–363. [CrossRef]
72. Ghazizadeh, A.; Haddadi, S.A.; Mahdavian, M. The effect of sol–gel surface modified silver nanoparticles on the protective properties of the epoxy coating. *RSC Adv.* **2016**, *6*, 18996–19006. [CrossRef]
73. Iannucci, L.; Parvis, M.; Sangermano, M.; Angelini, E.; Grassini, S. Rivestimenti ibridi organico-inorganici per la protezione dalla corrosione. *La Metall. Ital.* **2020**, *11*, 60–63.
74. Procaccini, R.; Bouchet, A.; Pastore, J.I.; Studdert, C.; Ceré, S.; Pellice, S. Silver-functionalized methyl-silica hybrid materials as antibacterial coatings on surgical-grade stainless steel. *Prog. Org. Coat.* **2016**, *97*, 28–36. [CrossRef]
75. Anghelone, M.; Jembrih-Simbürger, D.; Schreiner, M. Influence of phthalocyanine pigments on the photo-degradation of alkyd artists' paints under different conditions of artificial solar radiation. *Polym. Degrad. Stab.* **2016**, *134*, 157–168. [CrossRef]
76. Gulmine, J.; Janissek, P.; Heise, H.; Akcelrud, L. Degradation profile of polyethylene after artificial accelerated weathering. *Polym. Degrad. Stab.* **2003**, *79*, 385–397. [CrossRef]
77. Chiantore, O.; Trossarelli, L.; Lazzari, M. Photooxidative degradation of acrylic and methacrylic polymers. *Polymer* **2000**, *41*, 1657–1668. [CrossRef]
78. Kaczmarek, H.; Kamińska, A.; van Herk, A. Photooxidative degradation of poly (alkyl methacrylate) s. *Eur. Polym. J.* **2000**, *36*, 767–777. [CrossRef]
79. Mittelman, A.M.; Fortner, J.D.; Pennell, K.D. Effects of ultraviolet light on silver nanoparticle mobility and dissolution. *Environ. Sci. Nano* **2015**, *2*, 683–691. [CrossRef]
80. Odzak, N.; Kistler, D.; Sigg, L. Influence of daylight on the fate of silver and zinc oxide nanoparticles in natural aquatic environments. *Environ. Pollut.* **2017**, *226*, 1–11. [CrossRef]
81. Lin, C.-C.; Lin, D.-X.; Lin, S.-H. Degradation problem in silver nanowire transparent electrodes caused by ultraviolet exposure. *Nanotechnology* **2020**, *31*, 215705. [CrossRef]
82. *ASTM E308-18*; Standard Practice for Computing the Colors of Objectives by Using the CIE System. ASTM: West Conshohocken, PA, USA, 2018.
83. Hasani, M.; Mahdavian, M.; Yari, H.; Ramezanzadeh, B. Versatile protection of exterior coatings by the aid of graphene oxide nano-sheets; comparison with conventional UV absorbers. *Prog. Org. Coat.* **2018**, *116*, 90–101. [CrossRef]
84. Herley, P.J.; Prout, E. The thermal decomposition of silver oxide. *J. Am. Chem. Soc.* **1960**, *82*, 1540–1543. [CrossRef]